

Electronic Supplementary Information

Electrochemical reduction of nitrate to ammonia in a fluidized electrocatalysis system with oxygen vacancy-rich CuO_x nanoparticles

Jing Geng,^{†ab} Sihan Ji,^{†ab} Hui Xu,^{a,b} Cuijiao Zhao,^a Shengbo Zhang^{a*} and Haimin Zhang^{a*}

^a Key Laboratory of Materials Physics, Centre for Environmental and Energy Nanomaterials, Anhui Key Laboratory of Nanomaterials and Nanotechnology, Institute of Solid State Physics, HFIPS, Chinese Academy of Sciences, Hefei 230031, China. E-mail: shbzhang@issp.ac.cn, zhanghm@issp.ac.cn

^b University of Science and Technology of China, Hefei 230026, China.

[†]These authors contributed equally to this work.

1. Experimental section.

Materials: Cupric oxide, potassium nitrate, potassium nitrate- ^{15}N , ammonium sulfate- $^{15}\text{N}_2$, ammonium sulfate, sodium hydroxide, sodium nitroferricyanide dehydrate and N-(1-naphthyl) ethylenediamine dihydrochloride were purchased from Aladdin Ltd. (China). Potassium nitrites, boric acid, salicylic acid and sodium citrate dehydrate were purchased from Macklin Reagent Ltd. (China). Potassium hydroxide was purchased General Reagent Ltd. (China). The water used throughout all experiments was purified through a Millipore system. All chemicals were used as received without further purification.

Characterization: The crystalline structures of samples were identified by the X-ray diffraction analysis (XRD, Philips X'pert PRO) using Ni filtered monochromatic CuK α radiation ($\lambda_{\text{K}\alpha 1} = 1.5418 \text{ \AA}$) at 40 kV and 40 mA. Transmission electron microscope (TEM) images of samples were obtained using JEMARM 200F operating at an accelerating voltage of 200 kV. High-resolution transmission electron microscope (HRTEM) were obtained on a JEOL-2010 transmission electron microscope. X-ray photoelectron spectroscopy (XPS) analysis was performed on an ESCALAB 250 X-ray photoelectron spectrometer (Thermo, America) equipped with Al K α 1, 2 monochromatized radiations at 1486.6 eV X-ray source. The electron spin resonance (ESR) measurements were performed on Bruker EMX plus 10/12 (equipped with Oxford ESR910 Liquid Helium cryostat).

Synthesis of CuO_x nanoparticles solution: CuO_x nanoparticles solution was synthesized by laser fragmentation of raw CuO powders at room temperature. The laser source is a nanosecond pulsed Nd: YAG laser (splight-600 from Innolas) with wavelength of 1064 nm, pulse width 7 ns and single pulse laser energy 250 mJ. First, 4 mg commercial CuO powders were dissolved in 40 mL deionized water, and then the suspension was stirred and irradiated by nanosecond laser for 10 min at room temperature. Finally, the CuO_x nanoparticles solution was obtained with a color of bright brown.

Electrochemical measurement: All electrochemical measurements were performed on a CHI 660E electrochemical workstation (CH Instrumental Corporation, Shanghai, China) using a two-compartment cell, which was separated by Nafion 117 proton exchange membrane. Nafion membrane (Nafion 117) was protonated prior to the NtrRR experiments. First, the Nafion 117 was boiled in deionized water for 30 min, then in H₂O₂ for 1 h and subsequently in deionized water for another 1 h, then in 0.5 M H₂SO₄ for 2 h, and finally in deionized water for 5 h, all of which were treated at 80 °C. The synthesized CuO_x solution (4.0 mL, 0.4 mg) as the electrocatalyst was dispersed into 0.1 M KOH solution (41 mL) presence of 50 ppm KNO₃ in the cathodic compartment for NtrRR measurements. The anodic chamber contained 45 mL of 0.1 M KOH solution. A Hg/HgO electrode was used as the reference electrode and a Pt wire was used as the counter electrode. The polarization curves were measured with a scan rate of 5.0 mV s⁻¹ at room temperature and all polarization curves were obtained at the steady-state ones after several cycles. For NtrRR experiments, the potentiostatic test was conducted by continuously supplying Ar into the electrolyte under ambient conditions. In this work, all measured potentials (vs. Hg/HgO) were transformed into the potentials vs. reversible hydrogen electrode (RHE) based on the following equation:

$$E (\text{V vs. RHE}) = E (\text{V vs. Hg/HgO}) + 0.059 \times \text{pH} + 0.098$$

where E (V vs. RHE) is the converted potential (V) vs. RHE, E (V vs. Hg/HgO) is the experimentally measured potential against Hg/HgO reference electrode, 0.098 is the value of standard potential for the Hg/HgO reference electrode at 25 °C.

Determination of ammonia: Concentration of the produced ammonia was spectrophotometrically detected by the indophenol blue method. In detail, 5 mL of sample was taken, and then diluted with 5 mL of deionized water. Subsequently, 100 μL of oxidizing solution (sodium hypochlorite (pCl=4~4.9) and 0.75 M sodium hydroxide), 500 μL of colouring solution (0.4 M sodium salicylate and 0.32 M sodium hydroxide) and 100 μL of catalyst solution (0.1g Na₂[Fe(CN)₅NO]·2H₂O diluted to 10 mL with deionized water) were added respectively to the measured sample solution. After the placement of 1 h at room temperature, the absorbance

measurements were performed at wavelength of 697.5 nm. The obtained calibration curve was used to calculate the ammonia concentration.

Determination of NO_2^- : 20 g of p-aminobenzene sulfonamide was added to a mixed solution of 250 ml of water and 50 ml of phosphoric acid, and then 1 g of N-(1-naphthyl)-ethylenediamine dihydrochloride was dissolved in the above solution. Finally, the above solution was transferred to a 500 mL volumetric flask and diluted to the mark. Boric acid saturated solution was used to adjust the pH of electrolyte to weak acid. 1.0 mL electrolyte was taken out from the electrolytic cell and diluted to 5 mL with 3 mL boric acid saturated solution and 1 mL H_2O . Next, 0.1 mL color reagent was added into the above mentioned 5 mL solution. After shaking and standing for 20 minutes, the absorbance measurements were performed at wavelength of 540 nm. The obtained calibration curve was used to calculate the ammonia concentration.

Calculations.

The equation of NH_3 yield rate:

$$R(NH_3)(\mu g h^{-1} mg cat^{-1}) = \frac{C(NH_4^+ - N)(\mu g mL^{-1}) \times V(mL) \times 17}{t(h) \times m(mg) \times 14}$$

where $R(NH_3)$ is the ammonia yield rate; $C(NH_4^+-N)$ is the measured mass concentration of NH_4^+-N ; V is the electrolyte solution volume; t is the reaction time; 14 is the molar mass of NH_4^+-N atom; 17 is the molar mass of NH_3 molecules; m was the mass of catalysts (typically 0.4 mg).

The equation of Faradaic efficiency:

$$FE(NH_3)(\%) = \frac{8 \times n(NH_3)(mol) \times F}{Q} \times 100\%$$

where F is the Faradaic constant (96485.34); Q is the total charge during the NtrRR.

The equation of NO_2^- yield rate:

$$R(NO_2^-)(\mu g h^{-1} mg cat^{-1}) = \frac{C(NO_2^- - N)(\mu g mL^{-1}) \times V(mL) \times 46}{t(h) \times m(mg) \times 14}$$

where $R(NO_2^-)$ is the ammonia yield rate; $C(NO_2^--N)$ is the measured mass concentration of NO_2^--N ; V is the electrolyte solution volume; t is the reaction time;

14 is the molar mass of NO_2^- -N atom; 46 is the molar mass of NO_2^- molecules; m was the mass of catalysts (typically 0.4 mg).

The equation of Faradaic efficiency:

$$FE(\text{NO}_2^-)(\%) = \frac{2 \times n(\text{NO}_2^-)(\text{mol}) \times F}{Q} \times 100\%$$

where F is the Faradaic constant (96485.34); Q is the total charge during the NtrRR.

¹⁵N isotope labeling experiment: The ¹⁵N isotopic labeling experiments were conducted using 0.1 M KOH electrolyte containing 50 ppm K^{15}NO_3 (99 at.% of ¹⁵N). After the potentiostatic electrolysis at -0.25 V (vs. RHE) for 2 h, the pH value was adjusted to be weak acid using 0.5M H_2SO_4 . In this work, $(^{15}\text{NH}_4)_2\text{SO}_4$ as reference was dissolved in 0.1 M KOH solution ($\text{D}_2\text{O}/\text{H}_2\text{O}$ mixed solution, $V_{\text{D}_2\text{O}}:V_{\text{H}_2\text{O}}=1:4$) for ¹H NMR (nuclear magnetic resonance) measurements. The ¹H NMR spectra were obtained using superconducting Fourier transform nuclear magnetic resonance spectrometer (Bruker Avance-400).

2. Additional figures

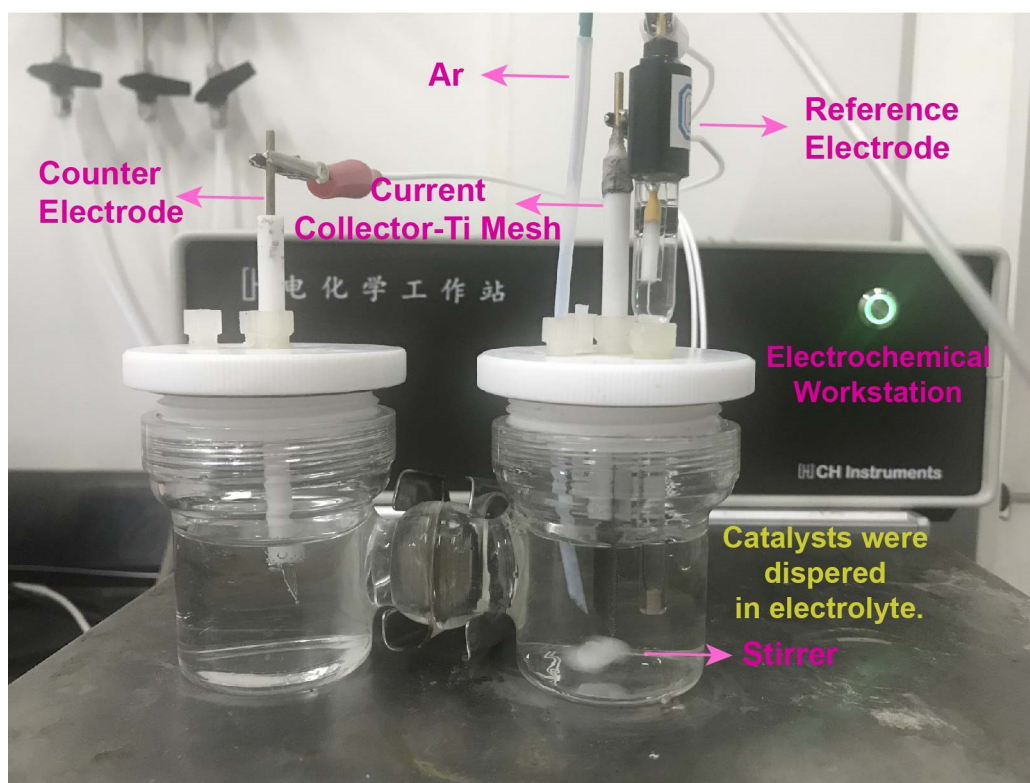


Fig. S1 A photograph of the fluidized electrocatalysis system setup in this work.

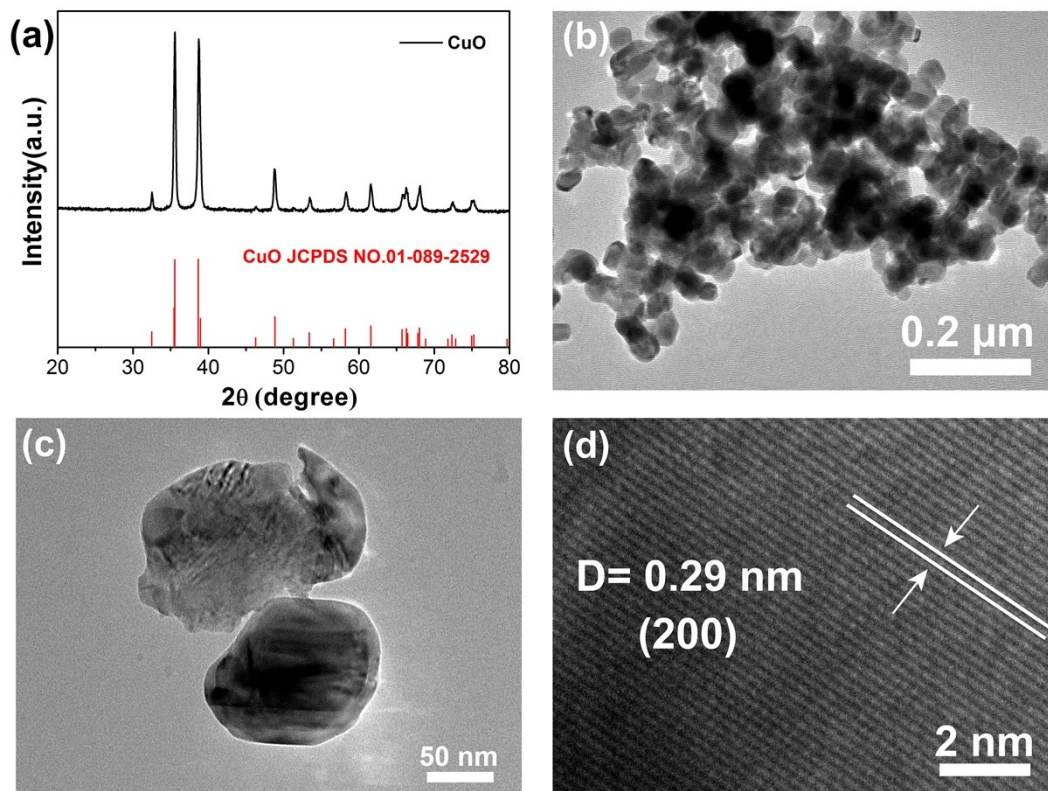


Fig. S2 (a) XRD patterns, (b, c) TEM images and (d) HRTEM image of CuO.

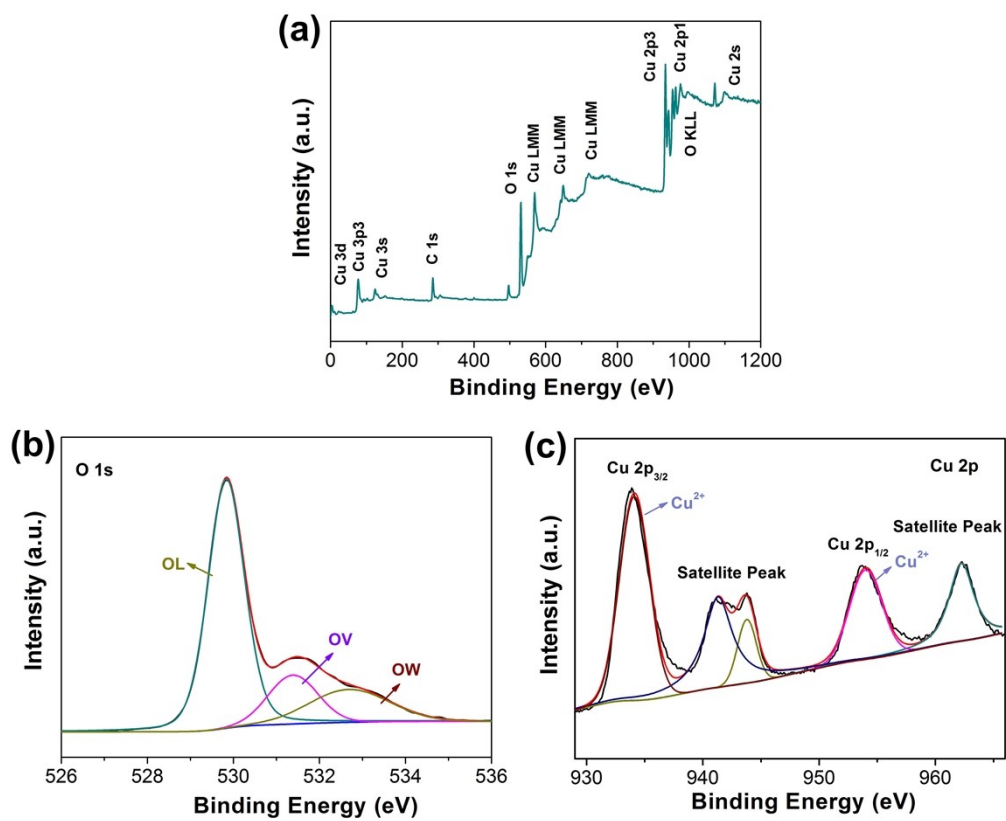


Fig. S3 XPS survey spectrum (a), O 1s (b) and Cu 2p (c) spectra of raw CuO.

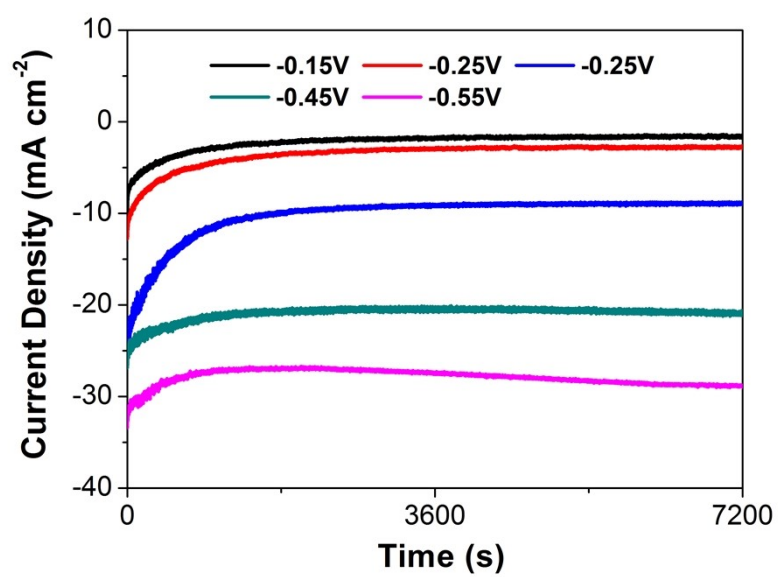


Fig. S4 The i - t curves of CuO_x nanoparticles catalyst for 2 h of NtrRR at various potentials (vs. RHE).

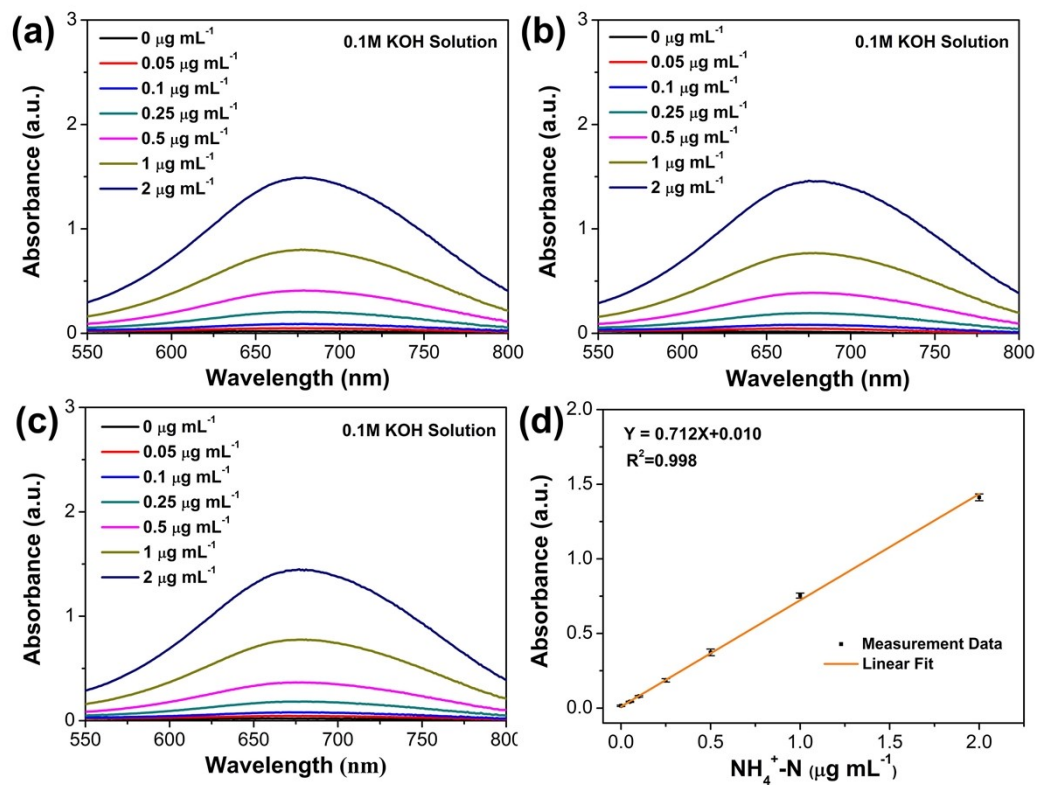


Fig. S5 (a), (b) and (c) UV/Vis absorption spectra of various NH_3 concentrations for three repeated experiments. (d) Calibration curve used for estimation of NH_3 concentration.

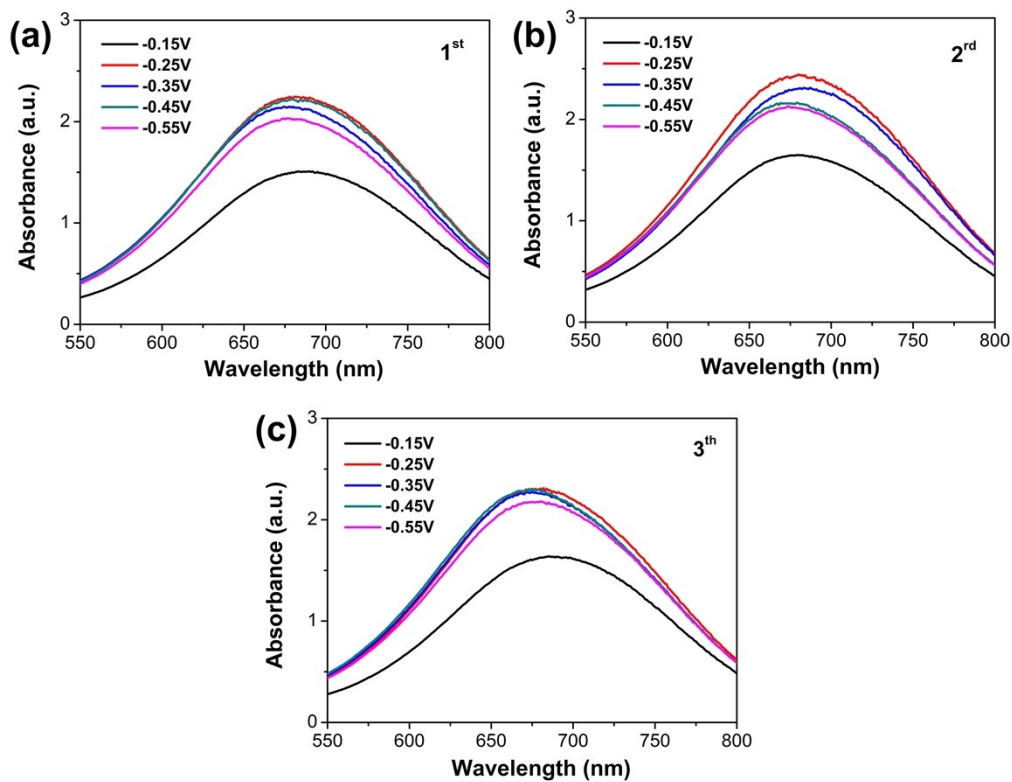


Fig. S6 UV-Vis absorption spectra of electrolytes stained with the indophenol indicator after NtrRR for 2 h for three repeated experiments.

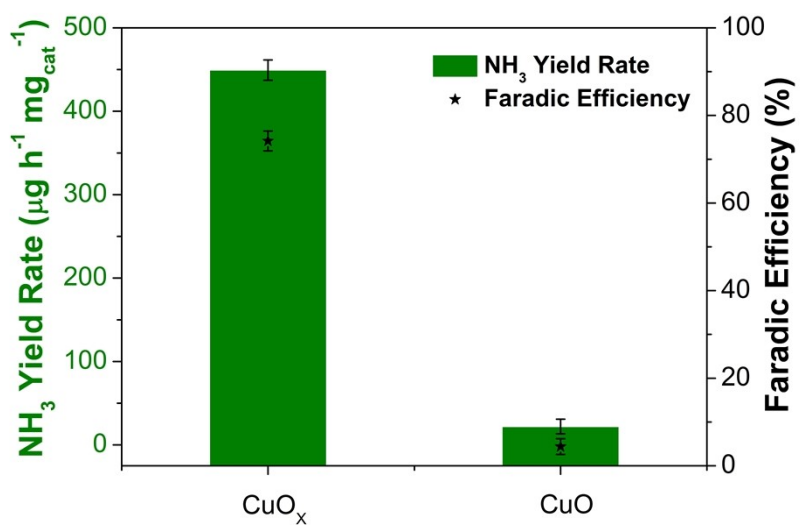


Fig. S7 NH₃ yield rate and FE of CuO_x and CuO at -0.25 V (vs. RHE) after 2 h of NtrRR in this fluidized electrocatalysis system. The error bars correspond to the standard deviations of three independent measurements.

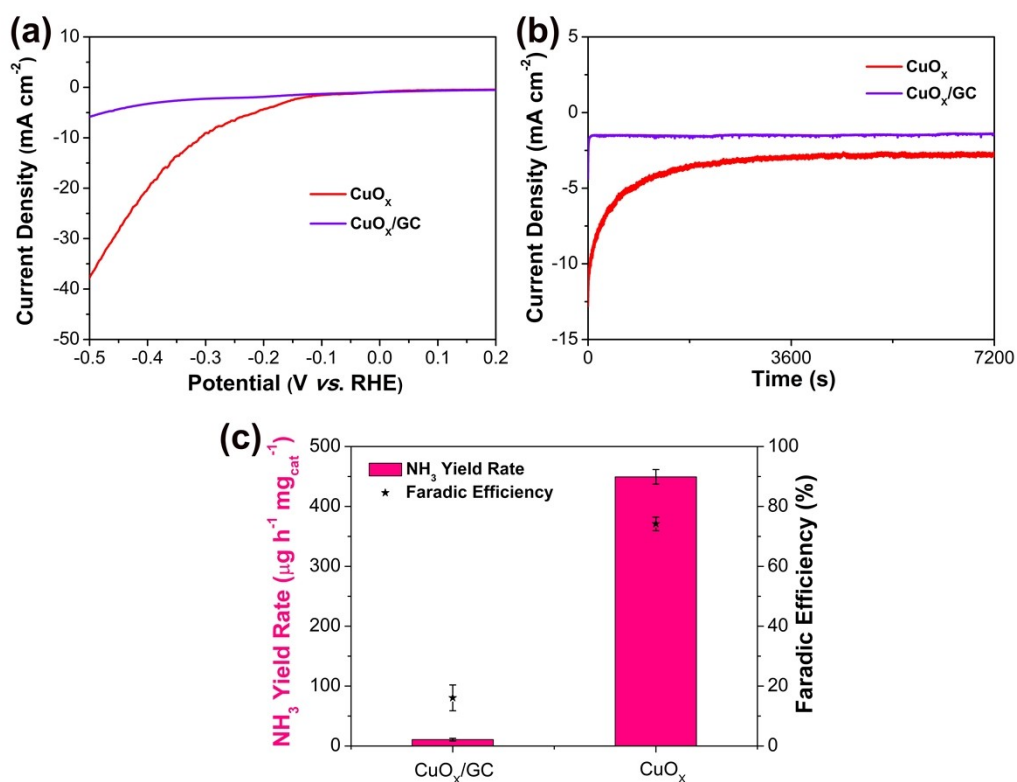


Fig. S8 (a) Linear sweep voltammetry curves of CuO_x/GC (GC: glassy carbon) in catalyst-loading system and CuO_x NPs in fluidized system. (b) The i-t curves of CuO_x/GC in catalyst-loading system and CuO_x NPs in fluidized system for 2 h of NtrRR at -0.25V (vs. RHE). (c) NH₃ yield rate and FE of CuO_x/GC in catalyst-loading system and CuO_x NPs in fluidized system at -0.25 V (vs. RHE) after 2 h of NtrRR.

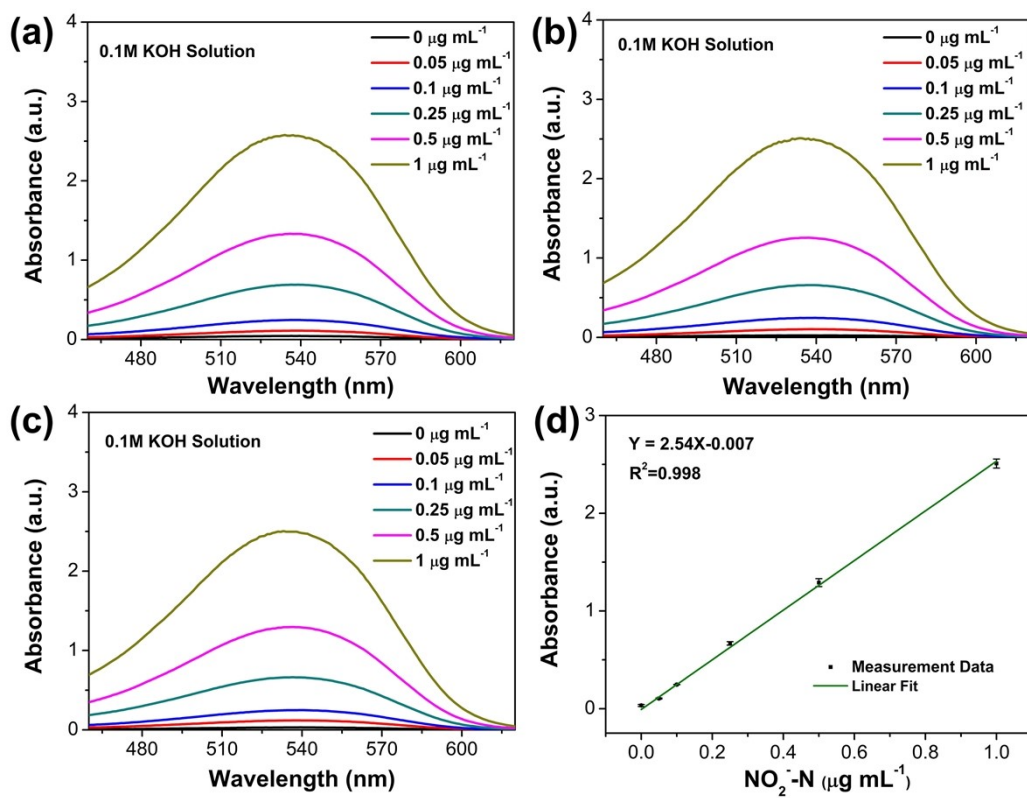


Fig. S9 (a), (b) and (c) UV/Vis absorption spectra of various NO_2^- concentrations for three repeated experiments. (d) Calibration curve used for estimation of NO_2^- concentration.

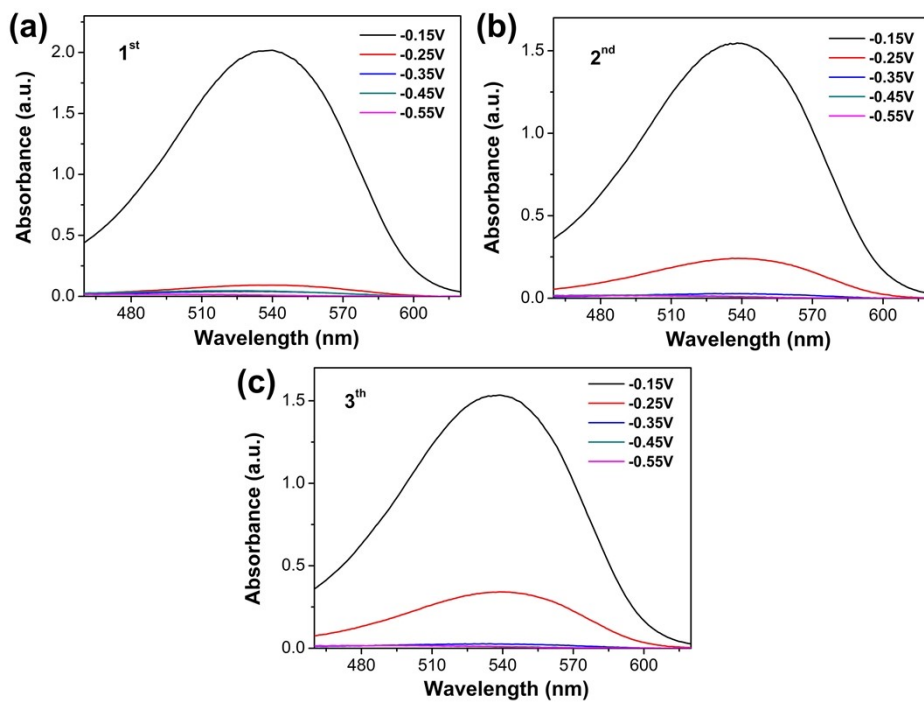


Fig. S10 UV-Vis absorption spectra of electrolytes stained with the Griess reagent after NtrRR for 2 h for three repeated experiments.

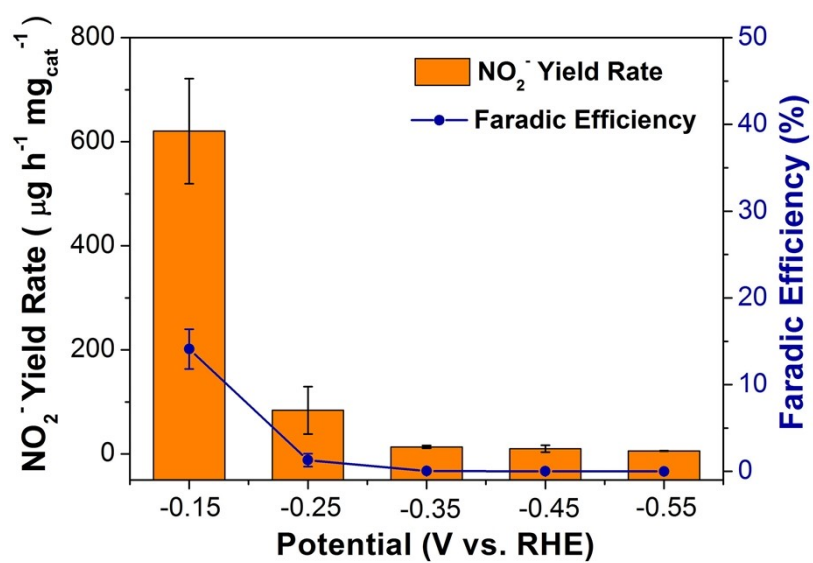


Fig. S11 NO₂⁻ yield rate and faradaic efficiency of CuO_x obtained at different potentials for 2 h NtrRR measurement. The error bars correspond to the standard deviations of three independent measurements.

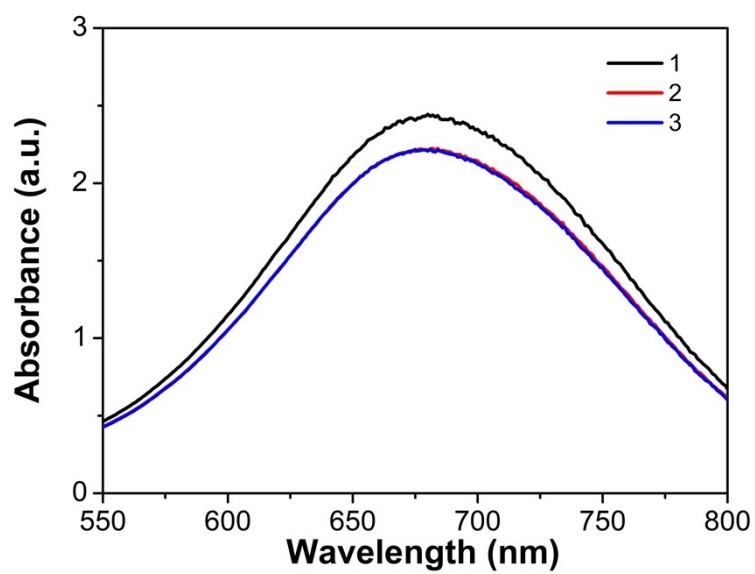


Fig. S12 UV-Vis absorption spectra of electrolytes (diluted 10 times) stained with the indophenol indicator after NtrRR for 10 h with three repeated experiments.

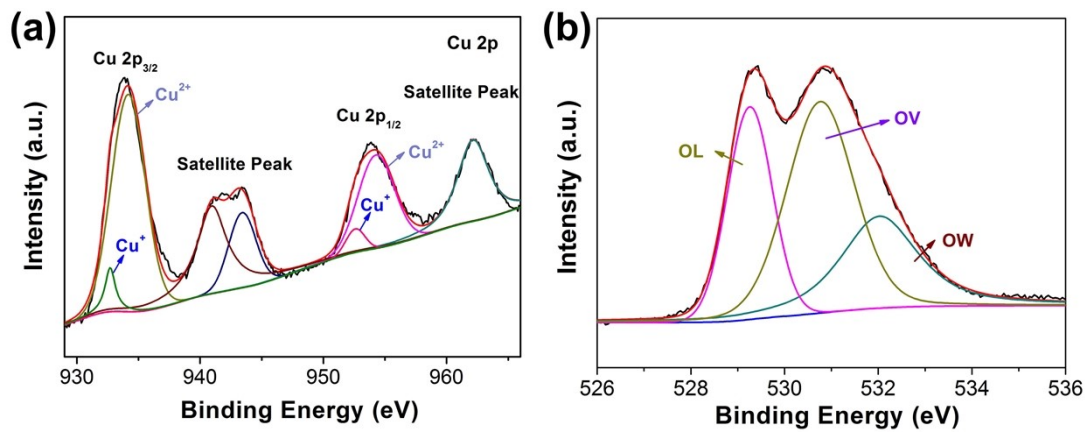


Fig. S13 The XPS spectra of Cu 2p (a) and O 1s (B) of CuO_x NPs after 10 h of NtrRR.

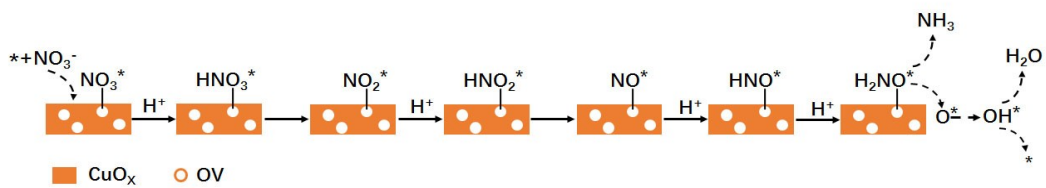


Fig. S14 The mechanism diagram to illustrate the role of oxygen vacancy in the nitrate reduction reaction.

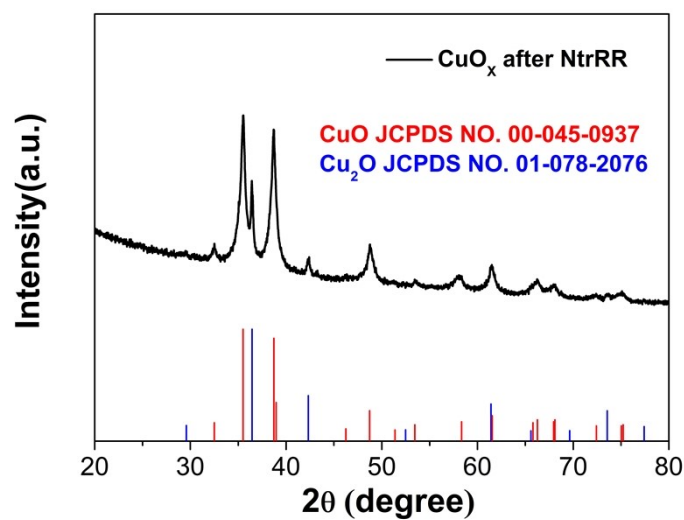


Fig. S15 XRD patterns of CuO_x after 10 h of NtrRR.

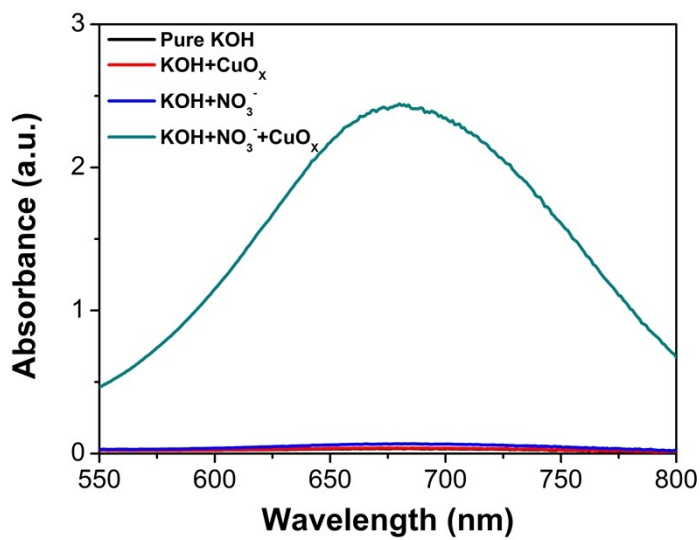


Fig. S16 Control experiments results. (a) pure KOH as the electrolyte, (b) KOH solution containing CuO_x catalyst as the electrolyte, (c) KOH solution with nitrate as the electrolyte, (d) KOH solution with nitrate containing CuO_x catalyst as the electrolyte. All the above tests were carried out in an Ar atmosphere, at -0.25 V (vs. RHE) for 2 hours.

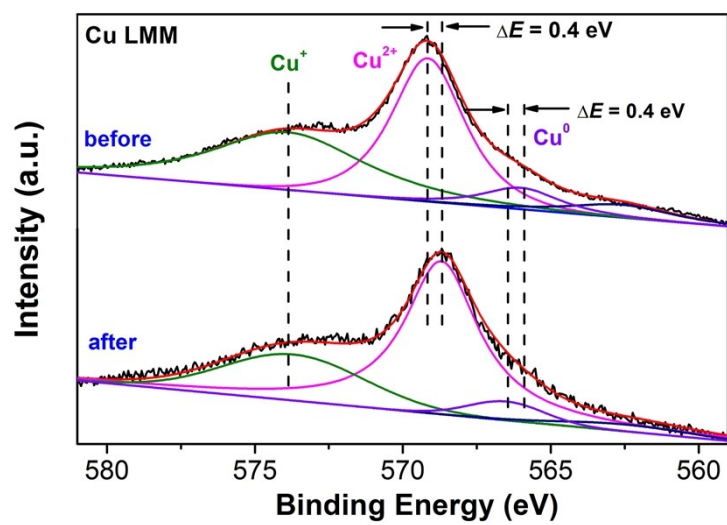


Fig. S17 Cu LMM AES spectra of CuO_x before and after 10 h of NtrRR.

Table S1. Comparison of the NtrRR performance of CuO_x electrocatalyst in this work and other electrocatalysts in reported literatures.

| Catalyst | Electrolyte | NH ₃ yield | FE (%) | Ref. |
|--|---|--|--------------|-----------|
| Ti foil | 0.4 M NO ₃ ⁻ | N/A | 82 | 1 |
| Cu-Ni alloy | 1 M KOH with 0.1 M KNO ₃ | 4160 μmol h ⁻¹ cm ⁻² | 99 | 2 |
| Fe-PPy SACs | 0.1 M KOH with 0.1 M KNO ₃ | 781.25 μg h ⁻¹ mg ⁻¹ | 100 | 3 |
| Cu/Cu ₂ O nanowire arrays | 0.5 M Na ₂ SO ₄ with 200-2000 ppm NaNO ₃ | 0.2449 mmol h ⁻¹ cm ⁻² | 95.8 | 4 |
| TiO ₂ nanotubes with oxygen vacancies | 0.5 M Na ₂ SO ₄ with 50-400 ppm NaNO ₃ | 810 μg h ⁻¹ mg ⁻¹ | 95.2 | 5 |
| Strained Ru nanoclusters | 1 M KOH with 1 M KNO ₃ | 1.0008*10 ⁸ μg h ⁻¹ mg ⁻¹ | ~100 | 6 |
| O-Cu-PTCDA | PBS with 500 ppm KNO ₃ | 67.07 ± 13.08 μg h ⁻¹ mg ⁻¹ | 77 ± 3 | 7 |
| Au/C | 0.5 M K ₂ SO ₄ with 1 mM KNO ₃ | 407.31 μg h ⁻¹ mg ⁻¹ | 26 | 8 |
| Cu/rGO/GP | 0.02 M NaCl with 0.02 M NO ₃ ⁻ | 0.0099 mmol h ⁻¹ cm ⁻² | N/A | 9 |
| Cobalt-tripeptide complex | 0.2 M citric acid with 0.1 M nitrite | N/A | 13.5 | 10 |
| Cu-Bi | 0.1 M Na ₂ SO ₄ with 100 ppm NO ₃ ⁻ | 0.0053 mmol h ⁻¹ cm ⁻² | N/A | 11 |
| Cu nanosheets | 0.1 M KOH with 10 mM KNO ₃ | 390.1 μg h ⁻¹ mg _{Cu} ⁻¹ | 99.7 | 12 |
| CuO _x nanoparticles | 0.1 M KOH with 50 ppm KNO ₃ | 449.41 ± 12.18 μg h ⁻¹ mg _{cat} ⁻¹ | 74.18 ± 2.27 | This work |

References

1. J. M. McEnaney, S. J. Blair, A. C. Nielander, J. A. Schwalbe, D. M. Koshy, M. Cargnello and T. F. Jaramillo, Electrolyte Engineering for Efficient Electrochemical Nitrate Reduction to Ammonia on a Titanium Electrode, *ACS Sustainable Chem. Eng.*, 2020, **8**(7), 2672–2681.
2. Y. Wang, A. Xu, Z. Wang, L. Huang, J. Li, F. Li, J. Wicks, M. Luo, D.-H. Nam, C.-S. Tan, Y. Ding, J. Wu, Y. Lum, C.-T. Dinh, D. Sinton, G. Zheng and E. H. Sargent, Enhanced Nitrate-to-Ammonia Activity on Copper–Nickel Alloys via Tuning of Intermediate Adsorption, *J. Am. Chem. Soc.*, 2020, **142**, 5702–5708.
3. Y. Xu, M. Z. Wang, K. L. Ren, T. L. Ren, M. Y. Liu, Z. Q. Wang, X. N. Li, L. Wang and H. J. Wang, Atomic defects in pothole-rich two-dimensional copper nanoplates triggering enhanced electrocatalytic selective nitrate-to-ammonia transformation, *J. Mater. Chem. A*, 2021, **9**, 16411–16417.
4. Y. T. Wang, W. Zhou, R. R. Jia, Y. Yu and B. Zhang, Unveiling the Activity Origin of a Copper-based Electrocatalyst for Selective Nitrate Reduction to Ammonia, *Angew. Chem. Int. Ed.*, 2020, **59**, 5350–5354.
5. R. R. Jia, Y. T. Wang, C. H. Wong, Y. F. Ling, Y. F. Yu and B. Zhang, Boosting Selective Nitrate Electroreduction to Ammonium by Constructing Oxygen Vacancies in TiO₂, *J. ACS Catal.*, 2020, **10**, 3533–3540.
6. J. Li, G. Zhan, J. Yang, F. Quan, C. Mao, Y. Liu, B. Wang, F. Lei, L. Li, A. W. M. Chan, L. Xu, Y. Shi, Y. Du, W. Hao, P. K. Wong, J. Wang, S. X. Dou, L. Zhang and J. C. Yu, Efficient Ammonia Electrosynthesis from Nitrate on Strained Ruthenium Nanoclusters, *J. Am. Chem. Soc.*, 2020, **142**, 7036–7046.
7. G. F. Chen, Y. Yuan, H. Jiang, S. Y. Ren, L. X. Ding, L. Ma, T. Wu, J. Lu and H. Wang, Electrochemical reduction of nitrate to ammonia via direct eight-electron transfer using a copper–molecular solid catalyst, *Nat. Energy*, 2020, **5**, 605–613.
8. J. Choi, H. L. Du, C. K. Nguyen, B. H. R. Suryanto, A. N. Simonov and D. R. MacFarlane, Electroreduction of Nitrates, Nitrites, and Gaseous Nitrogen Oxides: A Potential Source of Ammonia in Dinitrogen Reduction Studies, *ACS Energy Lett.*, 2020, **5**, 2095–2097.
9. D. Yin, Y. Y. Liu, P. F. Song, P. Chen, X. Liu, L. K. Cai and L. H. Zhang, In situ growth of copper/reduced graphene oxide on graphite surfaces for the electrocatalytic reduction of nitrate, *Electrochimica Acta*, 2019, **324**, 134846.
10. Y. X. Guo, J. R. Stroka, B. Kandemir, C. E. Dickerson and K. L. Bren, Cobalt Metallopeptide Electrocatalyst for the Selective Reduction of Nitrite to Ammonium, *J. Am. Chem. Soc.*, 2018, **140**, 16888–16892.
11. W. C. Gao, L. L. Gao, D. Li, K. T. Huang, L. Cui, J. Meng and J. Y. Liang, Removal of nitrate from water by the electrocatalytic denitrification on the Cu-Bi electrode, *J. Electroanal. Chem.*, 2018, **817**, 202–209.
12. X. B. Fu, X. G. Zhao, X. B. Hu, K. He, Y. N. Yu, T. Li, Q. Tu, X. Qian, Q. Yue, M. R. Wasielewski and Y. J. Kang, Alternative route for electrochemical ammonia synthesis by reduction of nitrate on copper nanosheets, *Appl. Mater. Today*, 2020, **19**, 100620.